Ramirez Hoyos, P.; Manzanares, JA.; Cervera Montesinos, J.; Gómez Lozano, V.; Ali, M.; Nasir, S.; Ensinger, W.... (2019). Surface charge regulation of functionalized conical nanopore conductance by divalent cations and anions. Electrochimica Acta. 325:1-7. https://doi.org/10.1016/j.electacta.2019.134914

Surface charge regulation of conical nanopore conductance by divalent cations and anions

Patricio Ramirez,[*,a] José A. Manzanares,[b] Javier Cervera,[b] Vicente Gomez,[a] Mubarak Ali,[c,d] Saima Nasir,[d] Wolfgang Ensinger,[d] and Salvador Mafe[*,b]

[a]*Departament de Física Aplicada, Universitat Politécnica de València, E-46022 València (Spain)*

[b]*Departament de Física de la Terra i Termodinàmica, Universitat de València, E-46100 Burjassot (Spain)*

[c]*Materials Research Department, GSI Helmholtzzentrum für Schwerionenforschung, D-64291 Darmstadt (Germany)*

[d]*Department of Material- and Geo-Sciences, Technische Universität Darmstadt, D-64287 Darmstadt (Germany)*

The surface charge regulation in nanoscale volumes is a subject of wide interest to biological and chemical soft matter systems. Also, electrolyte mixtures with monovalent and divalent ions are commonplace in practical applications with micro and nanoporous ion-exchange membranes. We have studied experimentally and theoretically the conductance of conical nanopores functionalized with negative and positive surface charges that are bathed by electrolyte mixtures of the monovalent ions K^+ and Cl^- and the divalent ions Mg^{2+}, Ba^{2+}, Ca^{2+}, and SO_4^{2-}. Small concentrations of these ions can modulate the nanopore selectivity and conductance because of their interaction with the charged groups on the pore surface. We have also given a qualitative description of the surface charge regulation using a simplified model for multivalent ion mixtures.

* **Corresponding authors**: E-mail addresses: patraho@fis.upv.es (P. Ramirez), smafe@uv.es (S. Mafe)

Keywords: functionalized conical nanopore, conductance minima, surface charge regulation, divalent ions

Graphical abstract

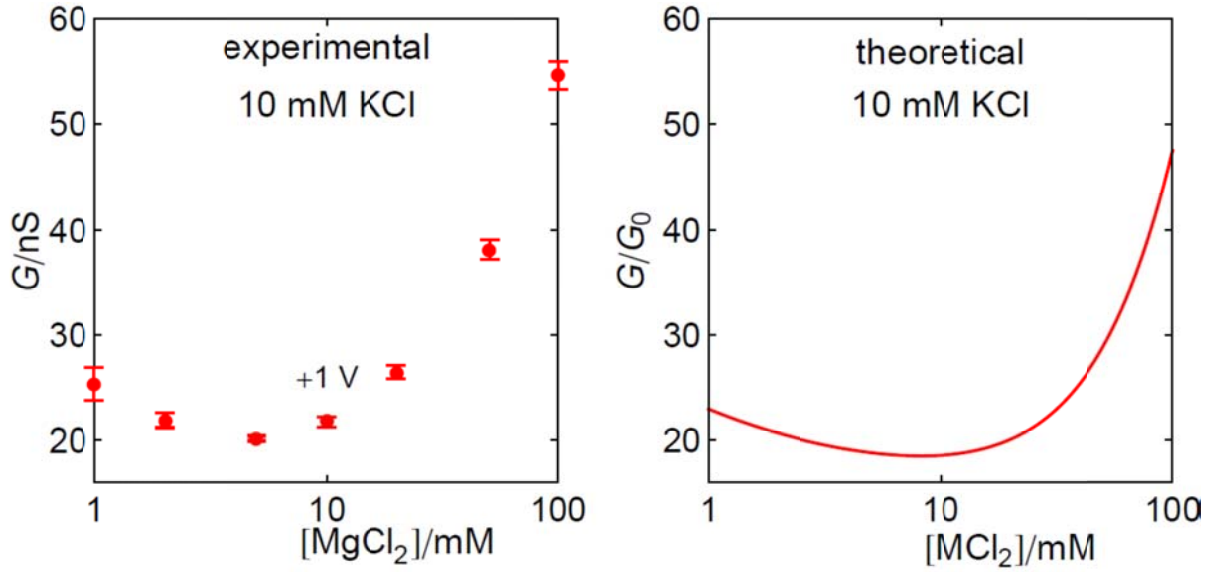

Surface charge regulation of nanopore conductance by divalent ions.

1. Introduction

Surface charge regulation by multivalent electrolytes is crucial to the electrophoresis of macromolecules such as DNA [1] and the conductance of the ion channel proteins in biological membranes that regulate physiological processes such as the cell cycle, tumorigenesis, and neuronal excitability [2–6].The external tuning of the pore surface charge density by mixtures of salts including divalent ions can modify also the ionic selectivity and conductance of artificial nanopores [7–10].

We report pore conductance data for a series of electrolyte mixtures containing the divalent ions Mg^{2+}, Ba^{2+}, Ca^{2+} and SO_4^{2-}. The conical nanopores are functionalized with negative or positive surface charges that strongly interact with the mobile divalent ions in the pore solution. The experimental data provide new physical insights on the surface charge regulation phenomena over nanoscale volumes and may suggest new applications in biosensing. The high surface-to-volume ratio typical of nanopores enhances the interaction of the mobile divalent ions with the pore charges and thus small concentrations of these ions in the electrolyte solution can modify the nanopore selectivity and conductance [10–13]. We have also presented theoretical calculations that qualitatively explain the observed phenomena.

The surface charge regulation of nanofluidic systems by salt mixtures is crucial in current biological and chemical problems [3,5,6,9,10]. For instance, magnesium and calcium cations are commonplace in biological cells and the carboxylic acid and amine groups at the pore surface are the chemical moieties found in most protein ion channels. Also, mixtures of asymmetric electrolytes with monovalent and divalent ions are typical in practical operations with ion-exchange [14] and solid-state [15] membranes.

2. Experimental

The membranes containing the single nanopores were obtained from stacks of 12.5 μm thick polyimide (PI) foils (Kapton50 HN, DuPont) that were irradiated at the *UNILAC* linear accelerator (GSI, Darmstadt) with Au swift heavy ions of energy 11.4 MeV per nucleon. In order to achieve single-ion irradiation, a metal mask with a 200 μm diameter centered aperture was located in front of the stack. The ion beam was immediately blocked after a single ion passed through the foil stack and was registered by a particle detector behind the samples. By using asymmetric track-etching techniques, the membrane tracks were converted into pores of approximately conical geometry [16–19]. SEM images of the nanopore fracture and gold replicas of the nanopores, together with nanopore conductance data, gave radii in the ranges 300–800 nm (base) and 10–40 nm (tip) [19]. Also, carboxylate residues were obtained at the pore surface because of the track-etching process. These pore groups are negatively charged in aqueous solutions at neutral pH [16,20]. The nanopore can also be functionalized with poly(allylamine hydrochloride) (PAH) or ethylene diamine chains by electrostatic or covalent attachment, respectively, which gives positively charged pore groups in aqueous solutions at neutral pH [21].

The input potential was a triangular wave signal. The resulting current was measured with a Keithley 6487 picoammeter (Keithley Instruments, Cleveland, Ohio). Aqueous solutions of mixtures of KCl and $MgCl_2$, $BaCl_2$, $CaCl_2$ or K_2SO_4 were used at approximately neutral pH values in the two bathing solutions, unless otherwise stated. Ag|AgCl electrodes were employed for the input potentials and output currents. The negatively-charged pore showed current-voltage curves characterized by high resistances when the current entered the cone base (negative voltages) and low resistances when the current entered the cone tip (positive voltages) [16,20], contrary to the case of the positively-charged pore.

3. Results and Discussion

3.1 Experimental data

The single-pore conductance $G = I/V$ shown in Fig. 1(a)–(d) is obtained at $V = 1$ V and 2 V for electrolyte mixtures involving a monovalent cation (K^+) and different divalent cations (Mg^{2+}, Ba^{2+} and Ca^{2+}) with a common anion (Cl^-) at pH = 7 approximately. Fig. 1(a) corresponds to the fixed 10 mM KCl concentration while the $MgCl_2$ concentrations are in the range $c_{MgCl_2} = 0$–100 mM. At low $MgCl_2$ concentrations, the conductance G decreases with increasing c_{MgCl_2} and reaches a minimum. Because this conduction regime is dominated by the pore surface charges [9,10,22], the conductance minimum suggests that the divalent cation Mg^{2+} strongly interacts with the negative carboxylic acid groups giving a decreased absolute value of the pore charge density. No evidence of pore charge inversion was however observed [23]. The interaction of the negative pore charges with divalent anions rather than cations has been studied previously [24]; no charge inversion occurs in this case because of the exclusion of the divalent ions from the pore solution.

For high $MgCl_2$ concentrations, G increases quasi-linearly with c_{MgCl_2} suggesting a bulk conduction regime regulated by the pore volume electroneutral solution [9,10,22]. In this regime, the surface charges are partially screened by the excess of mobile ions in the pore solution [25,26]. Note that the conductance minimum is not apparent for the case $V = -1$ V (Fig. 1(a), inset). This different behavior arises from the asymmetric geometry of the conical pore and the different concentration profiles that are obtained along the axial position for opposite pore directionalities [20].

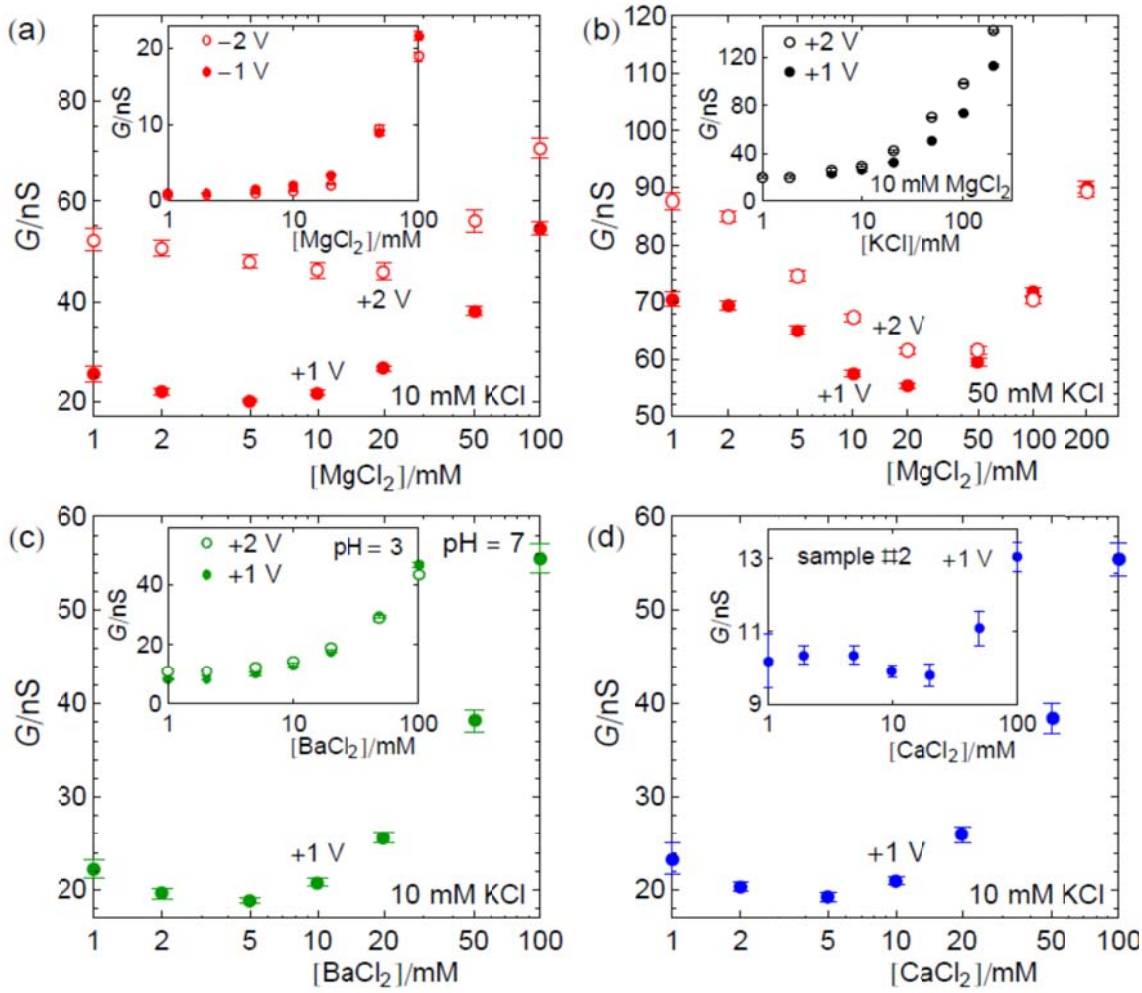

Fig. 1 (a) The experimental conductance–$MgCl_2$ concentration curve obtained at voltages $V = 1$ V and 2 V and 10 mM KCl. The inset corresponds to voltage $V = -1$ V and -2 V. (b) The conductance–$MgCl_2$ concentration curves obtained at voltages 1 V and 2 V and 50 mM KCl. The inset corresponds to the conductance–KCl concentration curves obtained at 10 mM $MgCl_2$ and voltages 1 V and 2 V. These latter curves practically overlap because the *I–V* curve is almost linear in this polarization regime. (c) The conductance–$BaCl_2$ concentration curve obtained at voltage $V = 1$ V and 10 mM KCl. The inset corresponds to pH = 3 (zero surface charge pore) and voltages 1 V and 2 V. (d) The conductance–$CaCl_2$ concentration curve obtained at 1 V and 10 mM KCl. The inset also corresponds to the conductance–$CaCl_2$ concentration curve obtained at 1 V and 10 mM KCl but now for a different conical nanopore with smaller radii. The error bars show the corresponding mean square deviations of three independent measurements. The voltage is applied at the cone tip side, as indicated in the experimental section.

In Fig. 1(b), the KCl concentration is fixed to 50 mM instead of 10 mM in Fig. 1(a). The minima in the G vs. c_{MgCl_2} curves are now shifted to higher concentrations with respect to Fig. 1(a) because the higher KCl concentration can screen more effectively the interaction between the divalent cations and the pore charges. Also, the inset of Fig. 1(b) shows that no minima are obtained in the G vs. c_{KCl} curves when we fix c_{MgCl_2} = 10 mM and it is the KCl concentration that is changed, emphasizing again the crucial role of the divalent cations in the surface charge regulation of the pore conductance. These results are in agreement with previous I–V curves showing that the positive currents and the pore rectification decrease at intermediate concentrations with respect to the values obtained at low Mg^{2+} concentrations [23].

The above results deviate significantly from the pore conductance observed in 1:1 electrolytes [25] and suggest that small amounts of divalent cations can decrease the effective pore charge. The resulting counter-intuitive effect is that the conductance decreases rather than increases with the salt concentration in the surface-regulated conductance regime, which is also confirmed here with other divalent cations. In Fig. 1(c), it is the Ba^{2+} cation that produces the minimum under experimental conditions similar to those of Fig. 1(a). Also, the inset suggests that the interaction of the negative pore charges with the divalent cations is crucial: no conductance minimum is observed at low pH value [7] because the carboxylic groups at the pore surface are not ionized. The cases of the Ca^{2+} cation in Fig. 1(d) and its inset show that the observed surface regulation phenomena are common to different salts and nanopores. Note also that the conductance minimum is shifted to higher concentrations for $V = 2$ V compared with the case of $V = 1$ V (Fig. 1(a)), consistent with the potential-dependent concentration profiles that occur along the axial position [20].

The conductance minima observed in Fig. 1(a), (c), and (d) can be characterized quantitatively [9,10]. In particular, G takes minimum values around 20 nS at a concentration

of *ca.* 5 mM for the divalent cation salts. In this conductance regime the value of G is dictated by the pore charges. Hence, the above minima can be roughly associated with significant decreases in the effective pore charge density with respect to the case of the lowest divalent cation concentration used. This experimental fact shows that the divalent cations can regulate the effective surface charges, and then the conductance of nanofluidic systems, at relatively low salt concentrations [2,9,10].

Similar conclusions have previously been obtained by other authors using different single-pore polymeric membranes [7] and solid-state nanochannels [10]. Also, the usual mole fraction experiments conducted in ion channel proteins have studied the current obtained with a mixture of two ions at constant total concentration in the external electrolyte solutions [2,7]. An anomalous mole fraction effect (AMFE) is observed when the current shows a minimum for a particular mole fraction [2,7]. While this minimum is usually ascribed to coordinated single filing effects due to the narrow pores characteristic of ion channels [6], other explanations invoke preferential binding of divalent over monovalent cations within the pore resulting in depletion zones of mobile ions (see Refs. 2, 7, 27, and 28 and references therein). We note that, for the relatively wide pores typical of most artificial nanopores, a systematic description of the AMFE phenomena have been given previously [7].

To better characterize the different pore conductance regimes, the case of aqueous mixtures composed of 10 mM KCl and 1 mM (Fig. 2(a)), 10 mM (Fig. 2(b)), 100 mM (Fig. 2(c)) and 200 mM (Fig. 2(d)) of $MgCl_2$, $CaCl_2$ and $BaCl_2$ have also been studied. Remarkably, opposite trends are obtained for the pore conductance order of the divalent cation salts at low and high concentrations in Fig. 2(a)–(d). We ascribe this reversal of the conductance order to the differences in the counterion hydration [22] and the distinct transport mechanisms characteristic of the surface and bulk regimes. In particular, we note that both the Pauling radii and the estimated water substitution rates around ions follow the increasing

order $Mg^{2+} < Ca^{2+} < Ba^{2+}$, while the hydration energies follow the decreasing order [6] $Mg^{2+} > Ca^{2+} > Ba^{2+}$.

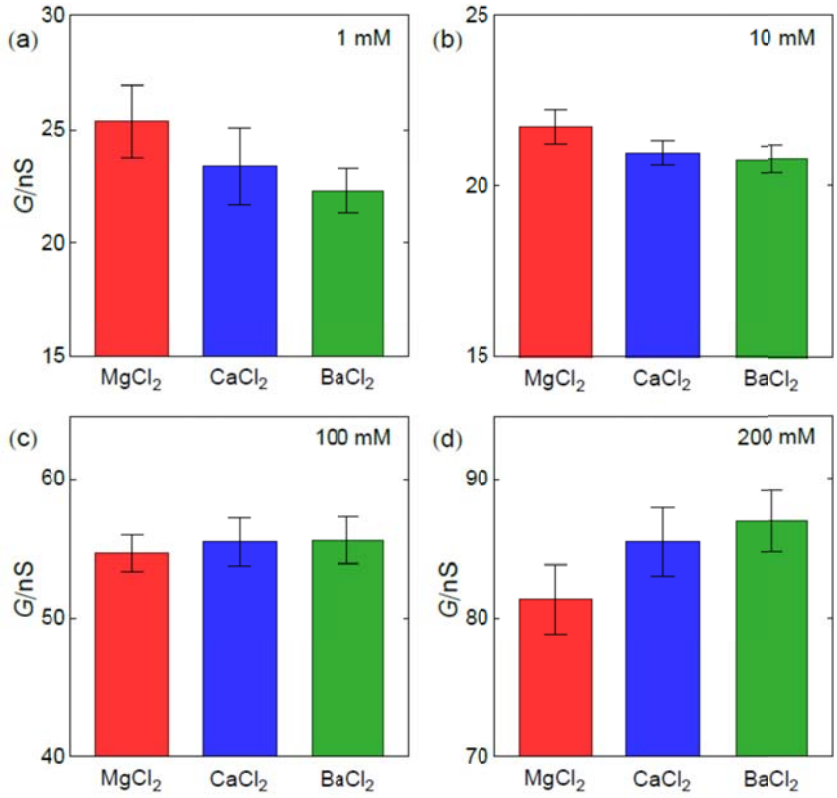

Fig. 2 Experimental pore conductances obtained at $V = 1$ V for aqueous mixtures of 10 mM KCl and (a) 1 mM, (b) 10 mM, (c) 100 mM, and (d) 200 mM of $MgCl_2$, $CaCl_2$ and $BaCl_2$. The error bars correspond to the mean square deviations of three independent measurements and clearly show the reproducibility and significance of the observed phenomena.

The above series suggest that the smaller naked counterion (Mg^{2+}) should be more hydrated than the larger naked counterion (Ba^{2+}). Thus, if surface conduction occurs without significant divalent cation dehydration, the retarding frictional force due to the electrostatic interaction with the pore charge groups would be stronger for the less hydrated cation (Ba^{2+}) having the lower hydration energy [22]. On the contrary, the strongly hydrated cation (Mg^{2+}) should be more retarded in the bulk conduction case because of the high hydrodynamic friction with the surrounding media. These opposite effects provide a qualitative

understanding [22] of the different results shown in Fig. 2(a)–(d) for the low concentration surface regime where $G(Mg^{2+}) > G(Ca^{2+}) > G(Ba^{2+})$ and the high concentration bulk regime where $G(Mg^{2+}) < G(Ca^{2+}) < G(Ba^{2+})$.

To check further the general nature of the observed phenomena, we studied also the conductance minima for the opposite case of divalent anions and a positively charged nanopore. To this end, aqueous electrolyte solutions with salt mixtures of KCl and K_2SO_4 were used. For the sake of comparison, Fig. 3(a) and (b) show the different I–V curves measured with positively (Fig. 3(a)) and negatively (Fig. 3(b)) charged pores for a series of monovalent and divalent ions. Note the different rectifications obtained for the two pore charges as well as the distinct behavior of monovalent and divalent ions. Although no evidence of pore charge inversion is observed in the I–V curves, the proximity of the divalent cations to the pore surface negative charges should decrease the effective value of this charge experienced by the counterions. We address this question in the modeling section [23].

Figures 3(c) and (d) show the pore conductances at $V = -1$ V and 1 V obtained with positive and negative pores, respectively, in the case of electrolyte mixtures involving monovalent (Cl^-) and a divalent (SO_4^{2-}) anions with a common cation (K^+) at pH = 7. The comparison of Fig. 3(c) with Fig. 1(a) and (b) shows that the conductance G also reaches a minimum for the positive pore and divalent anion both at positive and negative voltages. On the contrary, this minimum is not observed with the negative pore (Fig. 3(d)), as it could be expected due to the exclusion of the divalent anion from the pore solution in this case.

As observed for the divalent cation and the negatively charged pore, the existence of the conductance minimum in the case of the divalent anion and the positively charged pore (Fig. 3(c)) suggests that the divalent anion (SO_4^{2-}) strongly interacts with the respective oppositely charged surface groups giving a decreased absolute value of the pore charge.

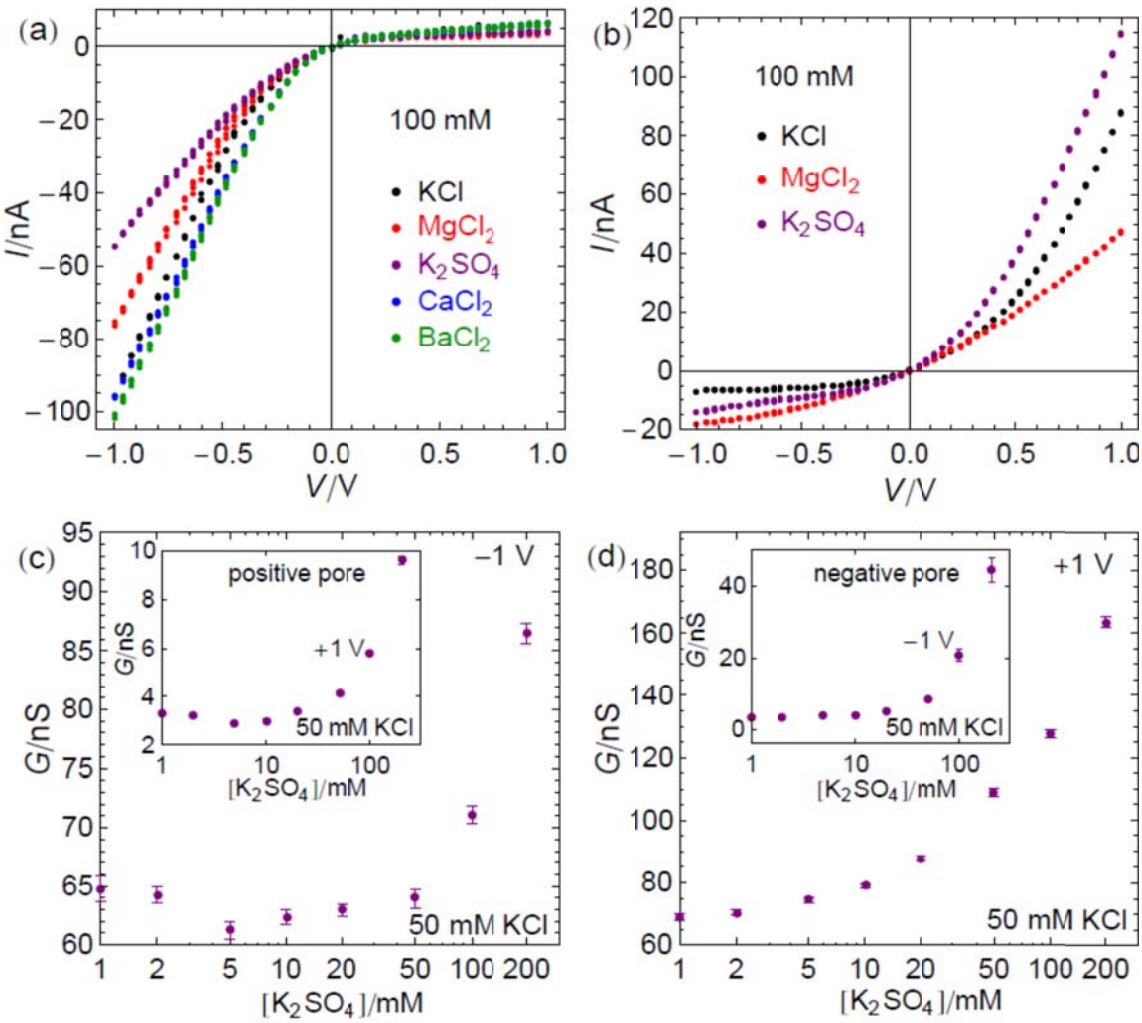

Fig. 3 (a) The experimental *I*–*V* curves for 100 mM KCl, $MgCl_2$, $CaCl_2$, $BaCl_2$, and K_2SO_4 solutions bathing the positively charged pore. (b) The experimental *I*–*V* curves for 100 mM KCl, $MgCl_2$, and K_2SO_4 solutions bathing the negatively charged pore. (c) The conductance–K_2SO_4 concentration curve obtained at fixed 50 mM KCl and the voltage $V = -1$ V for the positively charged pore. The inset corresponds to $V = 1$ V. (d) The conductance–K_2SO_4 concentration curve obtained at fixed 50 mM KCl and the voltage $V = 1$ V for the negatively charged pore. The inset corresponds to the voltage $V = -1$ V. In the *I*–*V* curves, the point sizes give an estimate of the experimental uncertainties.

We conducted new experiments with other additional samples to confirm further the results of Figs. 1 and 3 (see Figs. S1–S12 of the *Supporting Materials* file). In particular, we conducted a control experiment with solutions containing $MgCl_2$ only (no KCl added) and observed no conductance minima (Figs. S11 and S12).

3.2 Model results

A simple model can be used to analyze qualitatively the above experimental data. To allow a direct comparison with the salt concentrations used here, we use the equivalent volume concentration X_0 of fixed-charge groups rather than the surface charge density σ. This pore characteristic can be estimated from the local electroneutrality condition, which establishes that the mobile ion charge concentration must be equal to the equivalent fixed-charge concentration, which gives $X_0 = 2|\sigma|/(Fa)$ where a is the pore radius and F is the Faraday constant [20,22]. The concentration X_0 of fixed-charge groups is central to the Donnan distribution equilibria relating the external and pore ionic concentrations [22,29].

Consider an equivalent cylindrical pore of radius a and concentration X_0 of fixed-charge groups. Both compartments contain the same electrolyte mixture: a concentration c_1 of KCl and a concentration c_2 of a 2:1 electrolyte MCl_2, where M^{2+} is a generic divalent cation. The ionic species are denoted by subscripts i = 1 (K^+), 2 (M^{2+}), and 3 (Cl^-). The nanopore conductance G is proportional to the sum $\sum_{i=1}^{3} z_i^2 \bar{D}_i \bar{c}_i$ where the overbar indicates nanopore solution. Consistent with the qualitative nature of the model, we write its dimensionless value as

$$G/G_0 = (c_1/c_0)\mathrm{e}^{-\psi_\mathrm{D}} + 4D_\mathrm{r}(c_2/c_0)\mathrm{e}^{-2\psi_\mathrm{D}} + \left[(c_1+2c_2)/c_0\right]\mathrm{e}^{\psi_\mathrm{D}} \qquad (1)$$

where the reference conductance G_0 contains pore and solution general characteristics such as the radius a. To allow a comparison with the experimental results, the constant that scales the concentrations in Eq. (1) has been given the value c_0 = 7 mM. The divalent cation M^{2+} has a relative diffusion coefficient [30] $D_\mathrm{r} = \bar{D}_2/\bar{D}_3 \approx 0.25$ with respect to those of K^+ and Cl^-, $\bar{D}_1 \approx \bar{D}_3$. The ionic concentrations are calculated from the Donnan equilibrium distribution between the external and nanopore solutions [29]

$$\bar{c}_i = c_i \mathrm{e}^{-z_i \psi_\mathrm{D}} \tag{2}$$

where z_i is the charge number of ionic species i, $c_3 = c_1 + 2c_2$ as already used in Eq. (1), and ψ_D is the dimensionless Donnan potential, i.e., the Donnan potential scaled to RT/F, where R is the molar gas (or molar Boltzmann) constant and T is the thermodynamic temperature.

The divalent cations tend to accumulate in the vicinity of the negative charges at the pore surface so that they produce a decrease in the effective pore charge [31,32].This surface charge regulation is approximately described by the phenomenological equation

$$X = X_0 / (1 + K\bar{c}_2) \tag{3}$$

where X_0 is the value in absence of regulation and K is a binding constant. Equation (3) implicitly involves chemically-based adsorption and complex formation phenomena [31] rather than physically-based ionic pair correlation phenomena [32] to surface charge regulation (see Ref. 31 for a detailed comparison of these two approaches). We envisage here a transient ion-pair formation resulting in an effective pore charge of volume concentration $X < X_0$.

The dimensionless Donnan potential is calculated from the electroneutrality condition

$$c_1 \mathrm{e}^{-\psi_\mathrm{D}} + 2c_2 \mathrm{e}^{-2\psi_\mathrm{D}} - (c_1 + 2c_2)\mathrm{e}^{\psi_\mathrm{D}} = X \tag{4}$$

where X depends on ψ_D through $\bar{c}_2 = c_2 \mathrm{e}^{-2\psi_\mathrm{D}}$, as described by Eq. (3). Typical values of X_0 can be estimated as $2|\sigma|/(Fa)$ which gives concentrations in the range 100–1000 mM for charge densities in the range 0.1–1 e/nm^2 and radii in the range of nanometers, where F = 96 500 C/mol and e = 1.602 × 10^{-19} C. Thus, for the regulation of the pore surface charge to be significant at the divalent cation concentrations 10–50 mM used here, a scale value of the binding constant K should be of the order of 20–100 M^{-1} in Eq. (3). These values are close to the binding constant 100 M^{-1} found for magnesium binding to the carboxyl groups of the

bacterial porin *OmpF* [33] but significantly lower than those characteristic of calcium binding to the high-affinity moieties of typical ion channels, which are of the order of 10^4 M^{-1} [12].

Figures 4(a) and (b) show the results obtained by solving numerically Eqs. (1)–(4). These theoretical predictions at 10 mM and 50 mM KCl are in qualitative agreement with the experimental conductance curves of Fig. 1(a)–(d). The curves in the inset of Fig. 4(a) show the effects of decreasing the concentration $X_0 = 2|\sigma|/(Fa)$ on the conductance G. These curves qualitatively reproduce also the effects associated with the decrease of the pore charge density σ at low pH values (inset of Fig. 1(c)). Note also that for $V < 0$ the cations enter the cone base of high radio a_{base} instead of the low radio cone tip a_{tip} [20]. Thus, $X_{0,base} = 2|\sigma|/(Fa_{base}) < X_{0,tip} = 2|\sigma|/(Fa_{tip})$ for the two extreme charge concentration values of the conical pore, which could explain the absence of conductance minima in the case $V < 0$ (compare the inset of Fig. 4(a) with the inset of Fig. 1(a)). In addition, the experimental curve in the inset of Fig. 1(b) can also be compared with the theoretical curve in the inset of Fig. 4(b); note the absence of a conductance minimum in both cases.

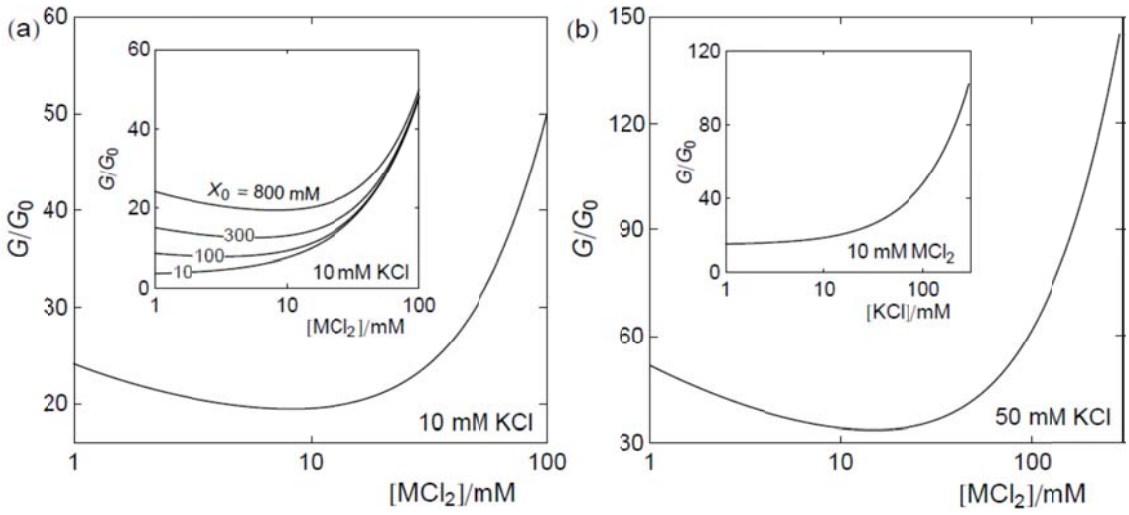

Fig. 4 (a) Calculated conductance vs. concentration of a 2:1 electrolyte at fixed 10 mM KCl. The values X_0 = 800 mM and $1/K$ = 30 mM are used in the calculations, unless otherwise stated. The inset corresponds to different values of $X_0 = 2|\sigma|/(Fa)$ simulating the experimental

conditions in the inset of Fig. 1(c) for a pH-dependent surface charge density σ. (b) At fixed 50 mM KCl, the minimum of the conductance curve is more pronounced. The inset shows that no minimum in the conductance curve as a function of the KCl concentration at fixed 10 mM of the generic 2:1 (MCl_2) electrolyte. Both predictions are in agreement with the experimental observations in Fig. 1.

The above results suggest that the conductance minima observed in our experiments do not arise because of the inhomogeneous electric field in the conical nanopores nor because of the fact that the equivalent charge concentration depends on the axial position (see, for example, Ref. [34]). Rather, the minima arise from the experimental fact that the divalent cations tend to accumulate in the vicinity of the negative charges at the pore surface so that they produce a decrease in the effective charge of narrow pores, regardless of the pore geometry.

4. Conclusions

We have provided new experimental data and physical insights concerning the surface charge-regulated conductance of a conical nanopore immersed in electrolyte mixtures of monovalent and divalent salts [7,9,10]. Small concentrations of Mg^{2+}, Ba^{2+}, Ca^{2+}, and SO_4^{2-} ions can allow the external tuning of the pore conductance due to their strong interaction with the charged groups at the pore surface. The experimental data of Fig. 1(a)–(d), Fig. 2(a)–(d), and Fig. 3(a)–(d) show surface charge regulation characteristics that should be of wide interest to biological and chemical processes occurring in nanoscale volumes [2,9,10,13–15]. We have also given a simple qualitative description of the observed phenomena that can now be extended for other multivalent ion mixtures. In particular, future work can now address other ionic selectivity effects concerning divalent ions by studying e.g. the pore reversal potential [10,35–37].

Conflicts of interest

There are no conflicts to declare.

Acknowledgments

P. R., J. C., J. A. M., V. G. and S. M. acknowledge the support from the Ministerio de Economia y Competitividad and European Regional Development Funds (project PGC2018-097359-B-100). M. A., S. N. and W. E. acknowledge the funding from the Hessen State Ministry of Higher Education, Research and the Arts, Germany, under the LOEWE project iNAPO.

References

[1] B. Luana, A. Aksimentiev, Electric and electrophoretic inversion of the DNA charge in multivalent electrolytes, *Soft Matter* 6 (2010) 243–246, https://doi.org/10.1039/B917973A.

[2] D. Gillespie, J. Giri, M. Fil, Reinterpreting the anomalous mole fraction effect: The ryanodine receptor case study, *Biophys. J.* 97 (2009) 2212–2221, https://doi.org/10.1016/j.bpj.2009.08.009.

[3] M. Levin, Reprogramming cells and tissue patterning via bioelectrical pathways: molecular mechanisms and biomedical opportunities, *Wiley Interdiscip. Rev.-Syst. Biol. Med.* 5 (2013) 657−676, https://doi.org/10.1002/wsbm.1236.

[4] J. Cervera, A. Pietak, M. Levin, S. Mafe, Bioelectrical coupling in multicellular domains regulated by gap junctions: a conceptual approach, *Bioelectrochem,* 123 (2018) 45–61, https://doi.org/10.1016/j.bioelechem.2018.04.013.

[5] M. Yang, W. J. Brackenbury, Membrane potential and cancer progression, *Front. Physiol.* 4 (2013) 185, https://doi.org/10.3389/fphys.2013.00185.

[6] B. Hille, *Ion Channels of Excitable Membranes*, Sinauer Associates, Sunderland, 1992.

[7] D. Gillespie, D. Boda, Y. He, P. Apel, Z. S. Siwy, Biophysical synthetic nanopores as a test case for ion channel theories: The anomalous mole fraction effect without single filing, *Biophys. J.* 95 (2008) 609–619, https://doi.org/10.1529/biophysj.107.127985.

[8] L. Benson, L.-H. Yeh, T.-H. Chou, S. Qian, Field effect regulation of Donnan potential and electrokinetic flow in a functionalized soft nanochannel, *Soft Matter* 9 (2013) 9767–9773, https://doi.org/10.1039/C3SM51981C.

[9] M. Fuest, K. K. Rangharajan, C. Boone, A. T. Conlisk, S. Prakash, Cation dependent surface charge regulation in gated nanofluidic devices, *Anal. Chem*. 89 (2017) 1593−1601, https://doi.org/10.1021/acs.analchem.6b03653.

[10] S. X. Li, W. Guan, B. Weiner, M. A. Reed, Direct observation of charge inversion in divalent nanofluidic devices, *Nanolett.* 15 (2015) 5046–5051, https://doi.org/10.1021/acs.nanolett.5b01115.

[11] Y. He, D. Gillespie, D. Boda, I. Vlassiouk, R. S. Eisenberg, Z. S. Siwy, Tuning transport properties of nanofluidic devices with local charge inversion, *J. Am. Chem. Soc.* 131 (2009) 5194–5202, https://doi.org/10.1021/ja808717u.

[12] M. Ali, S. Nasir, P. Ramirez, J. Cervera, S. Mafe, W. Ensinger, Calcium binding and ionic conduction in single conical nanopores with polyacid chains: Model and experiments, *ACS Nano* 6 (2012) 9247– 9257, https://doi.org/10.1021/nn303669g.

[13] H. Yao, Y. Cheng, J. Zeng, D. Mo, J. Duan, J. Liu, P. Zhai, Y. Sun, J. Liu, Bivalent ion transport through graphene/PET nanopore, *Appl. Phys. A* 122 (2016) 509, https://doi.org/10.1007/s00339-016-0021-z.

[14] S. Abdu, M.-C. Martí-Calatayud, J. E. Wong, M. García-Gabaldón, M. Wessling, Layer-by-layer modification of cation exchange membranes controls ion selectivity and water splitting, *ACS Appl. Mater. Interfaces* 6 (2014) 1843−1854, https://doi.org/10.1021/am4048317.

[15] D. Thiele, S. Kraszewski, S. Balme, F. Picaud, J.-M. Janota, P. Dejardin, Structure and ionic selectivity of a hybrid polyene/artificial polymer solid state membrane, *Soft Matter* 9 (2013) 684–691, https://doi.org/10.1039/C2SM26703A.

[16] Z. Siwy, D. Dobrev, R. Neumann, C. Trautmann, K. Voss, Electro-responsive asymmetric nanopores in polyimide with stable ion-current signal, *Appl. Phys. A* 76 (2003) 781–785, https://doi.org/10.1007/s00339-002-1982-7.

[17] P. Apel, Track etching technique in membrane technology, *Radiat. Meas.* 34 (2001) 559–566, https://doi.org/10.1016/S1350-4487(01)00228-1.

[18] M. Ali, B. Schiedt, K. Healy, R. Neumann, W. Ensinger, Modifying the surface charge of single track-etched conical nanopores in polyimide, *Nanotechnology* 19 (2008) 085713, https://doi.org/10.1088/0957-4484/19/8/085713.

[19] P. Ramirez, V. Garcia-Morales, V. Gomez, M. Ali, S. Nasir, W. Ensinger, S. Mafe, Hybrid circuits with nanofluidic diodes and load capacitors, *Phys. Rev. Applied* 7 (2017) 064035, https://doi.org/10.1103/PhysRevApplied.7.064035.

[20] J. Cervera, B. Schiedt, R. Neumann, S. Mafe, P. Ramirez, Ionic conduction, rectification, and selectivity in single conical nanopores, *J. Chem. Phys.* 124 (2006) 104706, https://doi.org/10.1063/1.2179797.

[21] M. Ali, B. Yameen, J. Cervera, P. Ramírez, R. Neumann, W. Ensinger, W. Knoll, O. Azzaroni, Layer-by-layer assembly of polyelectrolytes into ionic current rectifying solid-state nanopores: Insights from theory and experiment, *J. Am. Chem. Soc.* 132 (2010) 8338–8348, https://doi.org/10.1021/ja101014y.

[22] S. Mafe, J. A. Manzanares, P. Ramirez, Modeling of surface vs. bulk ionic conductivity in fixed charge membranes, *Phys. Chem. Chem. Phys.* 5 (2003) 376–383, https://doi.org/10.1039/B209438J.

[23] P. Ramirez, J. A. Manzanares, J. Cervera, V. Gomez, M. Ali, I. Pause, W. Ensinger, S. Mafe, Nanopore charge inversion and current-voltage curves in mixtures of asymmetric electrolytes, *J. Membrane Sci.* 563 (2018) 633–642, https://doi.org/10.1016/j.memsci.2018.06.032.

[24] G. Perez-Mitta, A. G. Albesa, M. E. Toimil Molares, C. Trautmann, O. Azzaroni, The influence of divalent anions on the rectification properties of nanofluidic diodes: Insights from experiments and theoretical simulations, *ChemPhysChem* 17 (2016) 2718–2725, https://doi.org/10.1002/cphc.20160037.

[25] G. B Westermann-Clark, J. L Anderson, Experimental verification of the space-charge model for electrokinetics in charged microporous membranes, *J. Electrochem. Soc.* 130 (1983) 839– 847, https://doi.org/10.1149/1.2119832.

[26] S. Mafé, P. Ramírez, A. Tanioka, J. Pellicer, Model for counterion-membrane-fixed ion pairing and Donnan equilibrium in charged membranes, *J. Phys. Chem.* 101 (1997) 1851–1856, https://doi.org/10.1021/jp962601b.

[27] W. Nonner, B. Eisenberg, Ion permeation and glutamate residues linked by Poisson-Nernst-Planck theory in L-type calcium channels, *Biophys. J.* 75 (1998) 1287–1305, https://doi.org/10.1016/S0006-3495(98)74048-2.

[28] W. Nonner, L. Catacuzzeno, B. Eisenberg, Binding and selectivity in L-type calcium channels: a mean spherical approximation, *Biophys. J.* 79 (2000) 1976–1992, https://doi.org/10.1016/S0006-3495(00)76446-0.

[29] K. Kontturi, L. Murtomäki, J. A. Manzanares, *Ionic Transport Processes: in Electrochemistry and Membrane Science*, Oxford University Press, Oxford, 2008.

[30] A. Goswami, A. Acharya, A. K. Pandey, Study of self-diffusion of monovalent and divalent cations in Nafion-117 ion-exchange membranes, *J. Phys. Chem. B* 105 (2001) 9196–9201, https://doi.org/10.1021/jp010529y.

[31] J. Lyklema, Overcharging, charge reversal: Chemistry or physics?, *Colloids Surf. A* 291 (2006) 3–12, https://doi.org/10.1016/j.colsurfa.2006.06.043.

[32] A. Y. Grosberg, T. T. Nguyen, B. I. Shklovskii, Colloquium: The physics of charge inversion in chemical and biological systems, *Rev. Mod. Phys.* 74 (2002) 329–345, https://doi.org/10.1103/RevModPhys.74.329.

[33] M. Queralt-Martin, E. García-Gimenez, S. Mafe, A. Alcaraz, Divalent cations reduce the pH sensitivity of OmpF channel inducing the pK_a shift of key acidic residues, *Phys. Chem. Chem. Phys.* 13 (2011) 563–569, https://doi.org/10.1039/c0cp01325k.

[34] J. Liu, D. Wang, M. Kvetny, W. Brown, Y. Li, G. Wang, Quantification of Steady-State Ion Transport through Single Conical Nanopores and a Nonuniform Distribution of Surface Charges, *Langmuir* 29 (2013) 8743–8752. https://doi.org/10.1021/la4009009.

[35] J. Cervera, A. Alcaraz, B. Schiedt, R. Neumann, P. Ramirez, Asymmetric selectivity of synthetic conical nanopores probed by reversal potential measurements, *J. Phys. Chem. C* 111 (2007) 12265–12273, https://doi.org/10.1021/jp071884c.

[36] A. H. Galama, J. W. Post, H. V. M. Hamelers, V. V. Nikonenko, P. M. Biesheuvel, On the origin of the membrane potential arising across densely charged ion exchange membranes: How well does the Teorell-Meyer-Sievers theory work?, *J. Membrane Sci. Res.* 2 (2016) 128–140, https://doi.org/10.22079/jmsr.2016.20311.

[37] A. Alcaraz, P. Ramirez, S. Mafe, H. Holdik, B. Bauer, Ion selectivity and water dissociation in polymer bipolar membranes studied by membrane potential and current–voltage measurements, *Polymer* 41 (2000) 6627–6634, https://doi.org/10.1016/S0032-3861(99)00886-1.